Computational Materials Science 50 (2011) 2872–2879

Contents lists available at ScienceDirect

Computational Materials Science

journal homepage: www.elsevier.com/locate/commatsci

Study of the hydrostatic pressure on orthorhombic IV–VI compounds including many-body effects

L. Makinistian *, E.A. Albanesi

INTEC-CONICET, Güemes 3450, 3000 Santa Fe, Argentina and Facultad de Ingeniería, Universidad Nacional de Entre Ríos, 3101 Oro Verde (ER), Argentina

ARTICLE INFO

Article history:
Received 28 December 2010
Received in revised form 19 April 2011
Accepted 1 May 2011
Available online 19 May 2011

Keywords:
Hydrostatic pressure
Optical properties
IV–VI orthorhombic compounds
GW correction
Electron–hole interaction

ABSTRACT

We performed a fully *ab initio* study of the relaxed volume optimization of the four orthorhombic IV–VI compounds (GeS, GeSe, α-SnS and SnSe), finding good agreement with experimental data from the literature. Based on the framework of the density functional theory and with a pseudopotential approach, we constructed the quasiparticle GW scheme to adjust the band structure and densities of states of the systems at different pressures, discussing the trends of the band gaps, that show metallization. Also, and within an effective two-particle equation for the response function, which includes the electron–hole interaction effects, we included the GW and the effective electron–hole contributions to the real and imaginary parts of the dielectric function and to the absorption coefficient of the four compounds both, at ambient and higher pressures. Comparison with experiments shows a satisfactory degree of agreement.

1. Introduction

High-pressure studies have long been an important area of solid state physics, specially since the development in the 1950s of the Diamond Anvil Cell (DAC), that made possible to generate pressures even above 100 GPa [1]. The issue of how electronic properties vary with pressure not only is of high interest on its own in the realm of pure Physics (e.g. Ref. [2]), but appears in cutting-edge applications such as high-pressure synthesis of materials [3], nanomaterials characterization [4], and high-pressure sensing [5], where the optical response to pressure has proven to be of paramount relevance [6].

In this work we study pressure effects on the orthorhombic IV–VI compounds – GeS, GeSe, α-SnS and SnSe – which have electronic and optical properties that make them attractive for their use in diverse technological applications such as cut-off devices and photovoltaic cells, and in the manufacture of infrared lasers [7–9] and detectors. Also, they have been studied for the evaluation of nanostructures etching [10]. In particular, SnS and SnSe have been used as shells for PbSe and PbS quantum dots, for the development of infrared-based devices [11], and as alternative for Cadmium in IR thin film coatings [12].

These compounds crystallize in an orthorhombic structure (*Pnma* 62 (D_{2h}^{16}) space group) and form double layers that are perpendicular to the direction of the unit cell largest axis. The unit cell contains eight atoms organized in two adjacent double layers. The atoms in each double layer bond to their three nearest neighbors and form a chain in zigzag along the direction of the minor axis of the crystal, see Fig. 1. The lattice parameters of the four compounds are presented in Table 1, where lattice parameters *a*, *b* and *c* – corresponding to the *x*, *y*, and *z* directions in the first Wigner–Seitz cell – are found along the parameters of the Murnaghan equation of state (see full discussion in Sections 2.1 and 3). Because of the dominant Van der Waals character of the bonds between adjacent layers, these materials cleave easily along the *b*–*c* (100) planes. All four orthorhombic IV–VI compounds have an intermediate behavior between a two dimensional and a three dimensional material.

These chalcogenides have been experimentally and theoretically assessed [13–30]. In particular, the pressure dependence of the structural parameters of these materials was studied [27–30] in experiments up to different pressures. It is to be remarked that *ab initio* constant pressure calculations [31,32] predict a *Pnma* → *Cmcm* phase transition for GeS at 35 GPa, and for SnS at ~4.5 GPa. These phase transitions have not yet been experimentally verified. Furthermore, in the case of SnS a pressure study [29] up to ~40 GPa shows no transition before ~18 GPa, where a first-order *Pnma* → $P2_1/c$ (monoclinic) is reported. Therefore, there is controversy regarding the phase diagram of SnS, and potentially of the rest of the IV–VI. In this work we model all systems using the experimental *Pnma* symmetry that, even in the case of SnS is expected to be a good approximation given the remarkably smooth second-order transition predicted in Ref. [32].

* Corresponding author.
E-mail addresses: lmakinistian@santafe-conicet.gov.ar (L. Makinistian), eaa@-santafe-conicet.gov.ar (E.A. Albanesi).

0927-0256/$ - see front matter © 2011 Elsevier B.V. All rights reserved.
doi:10.1016/j.commatsci.2011.05.002

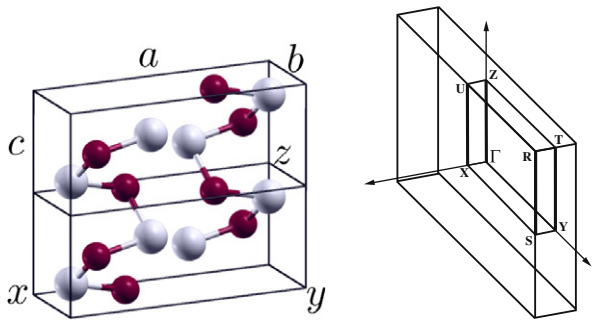

Fig. 1. Two unit cell of GeS (left) and the first Brillouin zone (right). The axes *x*, *y*, and *z* correspond to the lattice parameters *a*, *b*, and *c*, respectively. The cleavage plane is perpendicular to axis *x*. The unit cell for the other three compounds is very similar, differing only slightly in their dimensions (see Table 1).

In previous works [33–35] we performed studies on these compounds at ambient pressure, although neglecting the local field effects and the electron–hole interaction. Given the importance of the involvement of effective two-particle interactions, in this work we used the more sophisticated (and resource demanding) many-body approaches in order to further ensure the quality of our results. Here we provide with an unified *ab initio* treatment of the hydrostatic pressure to all four orthorhombic IV–VI compounds under pressure that, to the best of our knowledge, has not been published before: (i) a volume optimization study with relaxation of atomic positions, in an extended range of pressures (from ambient pressure to ~35 GPa), (ii) the calculation of the so called GW corrections [2,36–41] to the band gaps trend, with metallization ocurring upon increasing pressure, (iii) the calculation of optical properties consequently with (ii) variations, using the effective two-particle Bethe–Salpeter equation both, at ambient and higher pressures.

2. Computational details

2.1. Ground state electronic structure and volume optimization

We worked in the framework of the density functional theory (DFT) [42–44], using a plane-wave basis set using norm-conserving pseudopotentials method as implemented in the ABINIT package [45–47]. We used Trouiller-Martins type pseudopotentials implementing the Perdew–Burke–Ernzerhof (PBE) GGA parametrization scheme [48] as generated with the FHI98PP [49] code. The eigenvalues and eigenfunctions of the Kohn–Sham [50] equations were solved self-consistently using a $5 \times 10 \times 10$ Monkhorst and Pack [51] grid to sample the Brillion zone (BZ), and a 40 Ry cut-off energy for the wave functions. These parameters yielded a convergence of the total energy better than 10^{-4} Ry for the four compounds, and where used for the relaxation of atomic positions and the calculation of the densities of states and the band structures.

For each structure as well as for each pressure, we let the atomic positions relax to minimize internal forces: this probed indispensable to much better agree with the experimental data. In order to simulate hydrostatic pressure, when available, we used the lattice parameters found in the literature. It is to be remarked that the three lattice parameters change differently with pressure, thus a simultaneous variation by a given percentage to all of them would have not reproduced the effect of hydrostatic pressure. To fit the calculated energy vs. volume data, we evaluated three equations of states (EOS): the one by Teter et al. [52], the classical EOS by Murnaghan [53], and Birch–Murnaghan [54] EOS. Since the Murnaghan EOS best fits our results, we only report its $E(V)$ curve, and its negative volume derivative, $P(V) = -\frac{\partial E}{\partial V}(V)$.

2.2. Many-body treatement: GW and BSE

As it is well known, the local density approximation (LDA) for the exchange and correlation potential underestimates band gaps. This drawback, though sometimes less severe when other functionals such as GGA are used (e.g., Refs. [55–57]), is a common feature of ground state DFT and is due, at least partially, to the fact that the theory does not account for the electron–electron interaction. In order to include it in a description, Hedin [41,40] (see also, e.g., the thorough review by Onida et al. [38]) proposed the following quasiparticle eigen-equation:

$$\widehat{H}_0(\mathbf{r}_1)\psi(\mathbf{r}_1) + \int \Sigma(\mathbf{r}_1, \mathbf{r}_2, E)\psi(\mathbf{r}_2)d^3\mathbf{r}_2 = E\psi(\mathbf{r}_1) \quad (1)$$

where the interaction clearly comes as a perturbation to the non-interacting ground state hamiltonian, $\widehat{H}_0(\mathbf{r}_1) = T + V_N(\mathbf{r}_1) + V_{xc}(\mathbf{r}_1)$, that consists of the kinetic energy, the Hartree potential (i.e., Coulomb potential due to the nuclei), and the exchange-correlation (expressed as a functional of the electronic density, n_0). In Hedin's equation the so called self-energy operator, Σ, is non-local, non-hermitian, and energy-dependent. The fundamental building blocks [47] of the equations that Hedin proposed to find Σ are, besides Σ itself, the Green's function of the interacting many-body system, $G(\mathbf{r}_1, \mathbf{r}_2)$, the Green's function of an appropriate non-interacting system, $G_0(\mathbf{r}_1, \mathbf{r}_2)$, and the irreducible polarizability, $\tilde{\chi}(\mathbf{r}_1, \mathbf{r}_2) = -iGG$ which, through the inversed dielectric matrix $\varepsilon^{-1}(\mathbf{r}_1, \mathbf{r}_2) = 1 - v\tilde{\chi}$, re-normalizes the static (unscreened) Coulomb potential, $v(\mathbf{r}_1, \mathbf{r}_2) = \frac{e^2}{|\mathbf{r}_1 - \mathbf{r}_2|}$, resulting in the dynamical screened interaction $W(\mathbf{r}_1, \mathbf{r}_2) = \varepsilon^{-1}v$. Finally, the vertex function $\Upsilon(\mathbf{r}_1, \mathbf{r}_2, \mathbf{r}_3)$ describes the interactions between virtual holes and electrons, which is neglected in the so called GW method, yielding the self-energy operator as:

Table 1
Experimental ambient pressure volume and our parameters of the Murnaghan EOS. Where the lattice parameters are in Å, volumes are in Å^3, the energy E_0 is in eV, and the bulk moduli are in GPa.

	a	*b*	*c*	$V_{0_{exp}}$	BM fit on our calc.					$B_{0_{exp}}$	$B'_{0_{exp}}$
					V_0	E_0	B_0	B'_0	$^*B_{V_{0exp}}$		
GeS	10.495[a]	3.643[a]	4.305[a]	164.594	169.560	−1543.6	31.1	4.9	37.4		
GeSe	10.862[b]	3.862[b]	4.414[b]	185.163	190.920	− 1458.6	31.1	4.6	35.8	40.7 ± 3.5[b]	5.0 ± 0.4[b]
α-SnS	11.200[c]	3.987[c]	4.334[c]	193.532	199. 003	−1498.1	30.3	5.5	35.3	36.6(9)[c]	5.5(2)[c]
SnSe	11.4976[d]	4.1533[d]	4.440[d]	212.0232	218.858	−1413. 2	33.3	5.2	39.2		

[a] Ref. [27].
[b] Ref. [28].
[c] Ref. [29].
[d] Ref. [30].
* Estimation according to $B_{V_{0_{exp}}} = B_0 + B'_0 P(V_{0_{exp}})$, as in Ref. [66].

$$\Sigma(\mathbf{r}_1,\mathbf{r}_2,E)=\frac{i}{2\pi}\int G(\mathbf{r}_1,\mathbf{r}_2,E+E')W(\mathbf{r}_1,\mathbf{r}_2,E')dE' \quad (2)$$

We calculated GW corrections for the four compounds at the Γ point of the Brillion zone (BZ) (which contributes to defining the band gap) and used them as a uniform correction [58–63] to the conduction band of all the DOS and band structures we report in Section 3.2. For the GW calculations we used a $4\times6\times6$ Monkhorst and Pack [51] grid to sample the Brillion zone (BZ), a 20 Ry cut-off energy and 100 bands for the Kohn–Sham, and as usually acceptable, a lower cut-off energy for the expansion of the wave functions and the screening, 4 Ry for both, and 9 and 7 Ry for the wave functions and the self-energy, respectively. This set of parameters allowed a convergence of the GW corrections for the band gap better than 10 meV.

The GW corrections, which utilize the Kohn–Sham electronic structure together with the screened Coulomb interaction, were included in the Bethe–Salpeter equation (BSE) [64,38] to calculate the imaginary part of the dielectric function, ε_2, and included also in the other reported optical functions.

According to the BSE (see Eq. (4.12) in Ref. [38]), the macroscopic dielectric function considering electron–hole interaction is:

$$\varepsilon_M(\omega)=1-\lim_{\mathbf{q}\to0}\frac{4\pi e^2}{q^2}\sum_{\lambda}\frac{\left|\sum_{v,c}\langle v|e^{i\mathbf{q}\cdot\mathbf{r}}|c\rangle A_\lambda^{v,c}\right|^2}{\omega-E_\lambda+i\eta} \quad (3)$$

where $\mathbf{q}$ is a wave vector inside the Brillion zone (BZ), indexes v and c refer to valence and conduction bands respectively and E_λ and $A_\lambda^{v,c}$ are the eigenvalues and eigenvectors of $\widehat{H}^{exc}_{vc,v'c'}A^{v'c'}_\lambda=E_\lambda A^{vc}_\lambda$. The two-particle excitonic hamiltonian has three terms: $\widehat{H}^{exc}_{vc\mathbf{k};v'c'\mathbf{k}'}=\widehat{H}^{diag}_{vc\mathbf{k};v'c'\mathbf{k}'}+\widehat{H}^{exch}_{vc-\mathrm{fk};v'c'\mathbf{k}'}+\widehat{H}^{scr}_{vc\mathbf{k};v'c'\mathbf{k}'}$. The diagonal term accounts for the one particle-like photoabsorptive transitions and reads:

$$\widehat{H}^{diag}_{vc\mathbf{k};v'c'\mathbf{k}'}=(E_{c\mathbf{k}}-E_{v\mathbf{k}})\delta_{vv'}\delta_{cc'}\delta_{\mathbf{k}\mathbf{k}'} \quad (4)$$

The second term accounts for the so called electron–hole exchange, incorporating the bare Coulomb interaction, $\bar{v}$, which *does not* include the long range interaction (see $\mathbf{G}\neq0$ below), i.e., it describes the local field effects (due to the spatial variation of the density):

$$\begin{aligned}\widehat{H}^{exch}_{vc\mathbf{k};v'c'\mathbf{k}'}&=2\upsilon^{v'c'\mathbf{k}'}_{vc\mathbf{k}}\\&=2\frac{4\pi}{\Omega}\sum_{\mathbf{G}\neq0}\frac{1}{|\mathbf{G}|^2}\langle c\mathbf{k}|e^{i\mathbf{G}\cdot\mathbf{r}}|v\mathbf{k}\rangle\times\langle c'\mathbf{k}'|e^{-i\mathbf{G}\cdot\mathbf{r}}|v'\mathbf{k}'\rangle\end{aligned} \quad (5)$$

The third term takes care of the screening (due to the spatial variation of the self-energy) through ε_M^{-1}:

$$\begin{aligned}\widehat{H}^{scr}_{vc\mathbf{k};v'c'\mathbf{k}'}&=W^{v'c'\mathbf{k}'}_{vc\mathbf{k}}\\&=-\frac{4\pi}{\Omega}\sum_{\mathbf{G}\mathbf{G}'}\frac{\varepsilon^{-1}_{\mathbf{G}\mathbf{G}'}(\mathbf{q})}{|\mathbf{q}+\mathbf{G}|^2}\langle c\mathbf{k}|e^{i(\mathbf{q}+\mathbf{G})\cdot\mathbf{r}}|c'\mathbf{k}'\rangle\\&\quad\times\langle v'\mathbf{k}'|e^{-i(\mathbf{q}+\mathbf{G})\cdot\mathbf{r}}|v\mathbf{k}\rangle\delta_{\mathbf{q},\mathbf{k}-\mathbf{k}'}\end{aligned} \quad (6)$$

The $\mathbf{G}$ and $\mathbf{G}'$ are vectors of the reciprocal lattice. We used 24 bands (12 valence and 12 conduction) and, since the Haydock algorithm [65] implemented in ABINIT (chosen due to its smaller demand of computational resources) only calculates the imaginary part of the dielectric tensor, $Im[\varepsilon_M(\omega)]=\varepsilon_2(\omega)$, we computed the real part, $\varepsilon_1(\omega)$, from $\varepsilon_2(\omega)$ using the Kramers–Kronig relations in the form:

$$\varepsilon_1(\omega)_{\alpha\alpha}=1+\frac{2}{\pi}P\int_0^\infty\frac{\omega'\varepsilon_2(\omega')_{\alpha\alpha}}{\omega'^2-\omega^2}d\omega' \quad (7)$$

where P means the principal value of the integral. Finally, we also computed the absorption coefficient:

$$\alpha(\omega)_{\alpha\alpha}=\frac{2\omega}{c}\left(\frac{-\varepsilon_1(\omega)_{\alpha\alpha}+|\varepsilon(\omega)_{\alpha\alpha}|}{2}\right)^{\frac{1}{2}} \quad (8)$$

3. Discussion of results

3.1. Volume optimization

The top panel of Fig. 2 shows our calculated total energy vs. unit cell volume for GeS, GeSe, α-SnS and SnSe. We report results only on the orthorhombic phase of SnS (α-SnS), which suffers a phase transition into a monoclinic phase (γ-SnS) at 18.15 GPa [29]. All curves were referred to their corresponding E_0 so as to be plotted together in the same energy range: the highest energy increment is around 5 eV (~0.3% of E_0) for the highest pressures (~35 GPa for GeSe). In the bottom panel of the figure we plot our calculation of the pressure dependence of volume for the four systems, along with the available experimental data (none was found in the case of SnSe). A general feature is that our calculations overestimate the equilibrium volume around 3%: compare V_0 and $V_{0_{exp}}$ in Table 1. In the same Table, we stress that the calculated bulk moduli to be compared with the experimental ones are not the ones under the column "B_0" (31.1, 31.1, 30.3 and 33.3) but instead the ones under the column "$^*B_{V_{0_{exp}}}$" (37.4, 35.8, 35.3, and 39.2), calculated with the linear approximation expressed at the foot of the Table, as in Ref. [66]. The need of this correction comes from the overestimation of the equilibrium volumes that, in term, implies the assignment of a non-zero (positive) pressure to the experimental

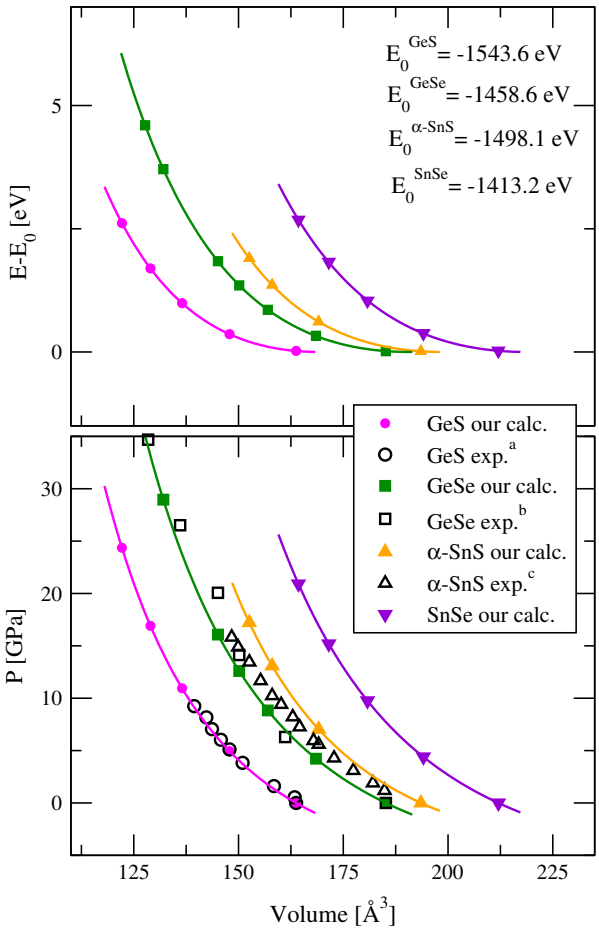

Fig. 2. Total energy and pressure as a function of unit cell volume. Continuous lines are the Murnaghan's EOS fit of our calculations. [a]Ref. [27], [b]Ref. [28], [c]Ref. [29].

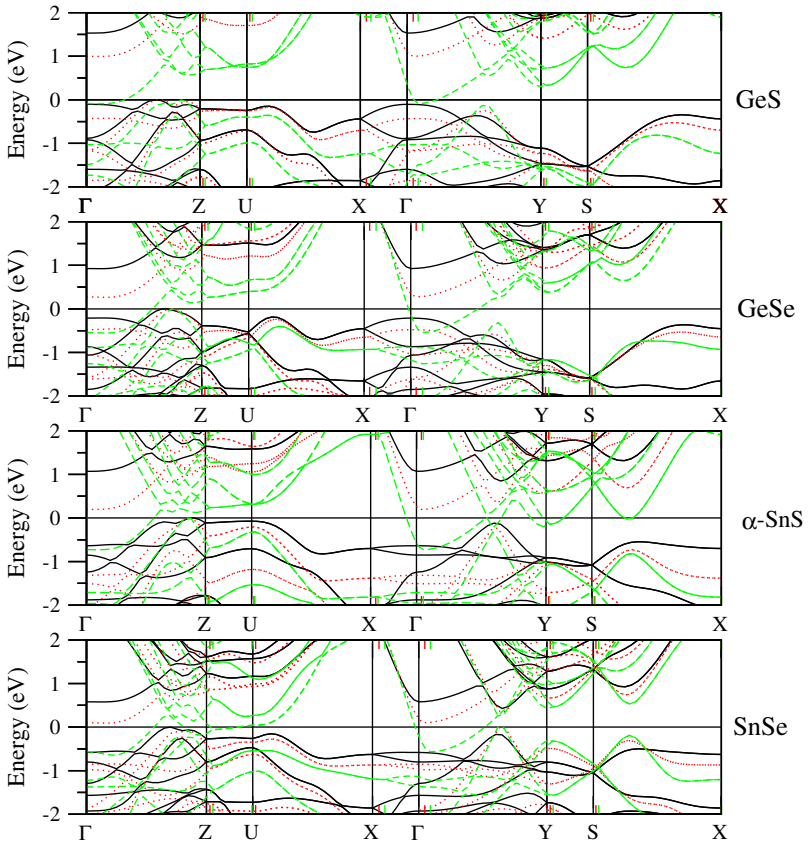

Fig. 3. Band structures for several pressures. In increasing order: continuous (lowest pressure), dotted (red online), dashed (green online, the highest pressure). Pressures, all in GPa, are the same as in Fig. 4: for GeS, ambient, 4.95, and 16.91; for GeSe, ambient, 4.23, and 12.60; for α-SnS, ambient, 7.03, and 13.09; for SnSe, ambient, 4.39, and 15.19. (For interpretation of the references to color in this figure legend, the reader is referred to the web version of this article.)

volume ($V_{0_{exp}}$) with no pressure applied (we call it $P(V_{0_{exp}})$). In the bottom panel of Fig. 2, and in the following sections we take as reference the experimental "zero pressure" (i.e., ambient pressure), meaning that we substract $P(V_{0_{exp}})$ to the calculated pressures of Fig. 2 so as to label "0 GPa" our calculations made with the experimental "zero pressure" lattice parameters. Our results slightly overestimate the equilibrium volume and underestimate the bulk moduli, which is a typical behavior of GGA–PBE calculations [67]. In spite of this, the trend of our curves follows the experimental data quite satisfactorily, in particular for GeS and GeSe; and our calculated $B_{V_{0_{exp}}}$ also are close to the experimental $B_{0_{exp}}$, most specially for α-SnS.

3.2. Electronic structure

3.2.1. Energy bands

Fig. 3 shows our calculated energy bands. We have plotted them along a normalized k-path in the first Brillouin Zone, so that bands for different pressures would span along the whole (and same) plotting range. Otherwise, different pressures and so different unit cell volumes, would force Brillouin Zones of different sizes making difficult the comparison among them. It is to be noticed that upon this normalization of the k-axis, the high symmetry points (Γ, Z, U, X, etc.) do not exactly coincide but rather fall near each other.

In Fig. 3, labels correspond to zero pressure and only the ticks for the high symmetry points for the higher pressures are plotted (color online, the higher the pressure, the more to the right the corresponding tick). At zero pressure, bands for GeS and GeSe are in general similar to each other. They both have an indirect gap in $\Gamma \rightarrow Z$ and a greater (∼0.15 eV) competing direct gap in Γ. Bands for α-SnS also show an indirect gap in $\Gamma \rightarrow Z$ and one almost direct in $\Gamma \rightarrow Y \sim 0.1$ eV greater. A similar behavior is seen for SnSe.

Our calculated gaps with and without the GW corrections, all of which we found indirect and in the $\Gamma \rightarrow$ Z direction of the Brillion zone (BZ), are presented in Table 2, along with the ranges of experimental gaps for ambient pressure found in the literature: it can be seen that the agreement for zero pressure is excellent except for the GeSe and SnSe, for which even with the GW correction we underestimate the band gap. This suggests that the PBE–GGA that we used for the ground state calculation underestimates the band gap too severely for the perturbative GW method to correct it. With regards to the selenides' gaps being more underestimated than those of the sulfides, this is a trend also found in the literature. For example, Vogel et al. [68] studied II–VI compounds and found the very same effect (being the underestimation for the tellurides even worse than the one for the selenides and the sulfides). The authors suggest that this is closely related to the inaccurate description of the strongly localized semicore d-electrons with an underestimation of their binding energies. This indeed could account for our results, given that the presence of semicore d-electrons in Selenium is a crucial difference with Sulphur. As pressure rises the valence and conduction band approach each other (i.e., metallization occurs): the gap decreases until it disappears when the bands overlap in energy, but do not cross, thus yielding a semimetalllic behavior.

Our calculations also suggest that even at the highest pressures we evaluated, the four systems remain semiconducting in the $\Gamma \rightarrow$ X direction (i.e., perpendicular to the easy-cleavage planes), indicating that conduction perpendicular to the bi-layers still presents a gap.

Table 2
Energy band gaps as a function of pressure.

	Pressure (GPa)	Band gap (eV)		
		E_g^0	E_g^{GW}	$E_g^{Expt.}$
GeS	0	1.09	1.53	1.35–2.04[a]
	4.95	0.62	1.00	
	16.91	Semimetal		
GeSe	0	0.68	0.93	1.07–1.29[b]
	4.23	0.08	0.26	
	12.60	Semimetal		
α-SnS	0	0.69	1.07	1.049–1.600[c]
	7.03	0.00	0.28	
	13.09	Semimetal		
SnSe	0	0.42	0.58	0.889–1.238[d]
	4.39	0.00	0.10	
	15.19	Semimetal		

[a] See Table 2 in Ref. [33].
[b] See Table 2 in Ref. [34].
[c] See Table 1 in Ref. [69].
[d] See Table 2 in Ref. [69].

3.2.2. Densities of states

In what follows, we make a general description of the DOS in terms of the cation (Ge and Sn) and the anion (S and Se), unless specific reference is needed (see Fig. 4). At zero pressure four main structures (three making the valence band and a forth constituting the conduction band) can be identified in the total DOS: a sharp peak at ∼−12.5 eV due to anion-*s* orbitals; a broader structure between −9.0 and −5.5 eV (for the two tin compounds), and between −8.7 and −5.2 eV (for the two Ge compounds) mainly due to cation-*s* orbitals with a smaller contribution of anion-*p* orbitals; another broad structure up to the fermi energy ($E_F = 0$ eV in our plots) mainly due to anion-*p* orbitals, but also cation-*p* orbitals and, cation-*s* orbitals, which in fact make the mayor contribution to the formation of the top of the valence band; and a broad structure as the conduction band, mainly due to *p*-orbitals from both the cation and the anion. As pressure rises, metallization occurs, in agreement with a previous prediction for GeS [31]. Also, the four structures in the densities of states for all four compounds stretch downwards in energy becoming broader and with decreasing amplitude of the peaks. The fermi surface is dominated by cation-*s* electrons, *p*-orbitals from both elements, and a minor though not neglectable contribution of anion-*d* orbitals.

3.3. Optical properties

Figs. 5–8 present our calculated real (ε_1) and imaginary (ε_2) parts of the dielectric function, and the absorption coefficient (α) for GeS, GeSe, α-SnS, and SnSe, respectively, for zero and higher pressures, and for light polarized in the three main axes of the crystal (*x*, *y*, and *z*, corresponding to the lattice parameters *a*, *b*, and *c*, respectively).

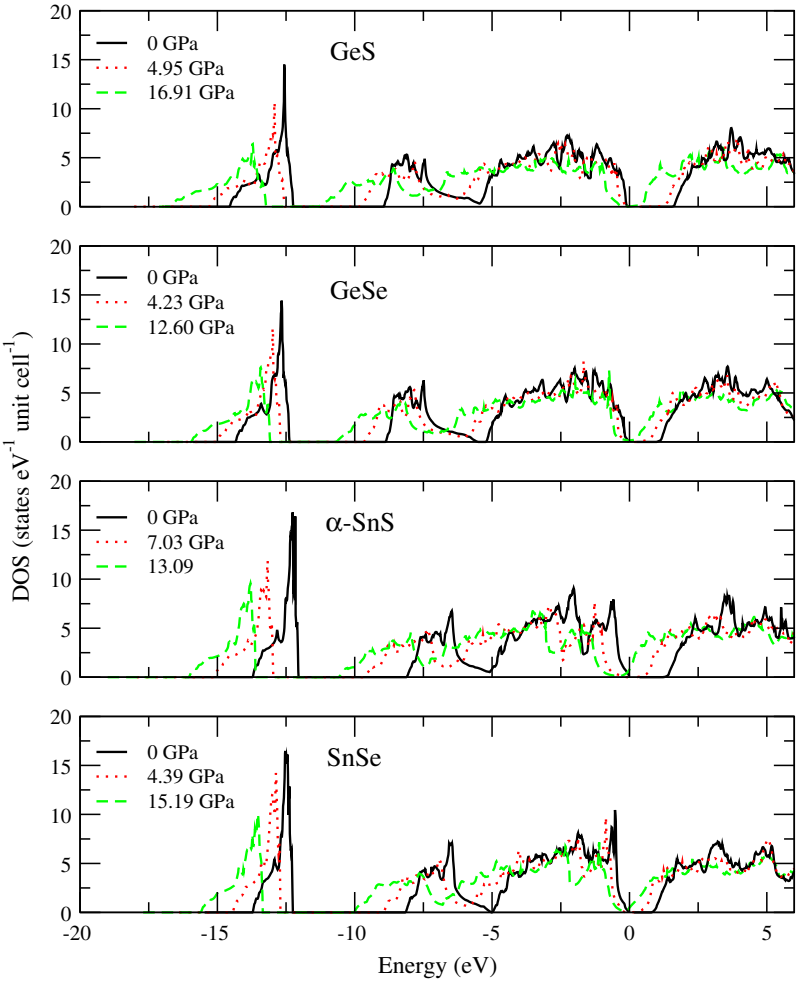

Fig. 4. Total densities of states of GeS, GeSe, α-SnS, and SnSe.

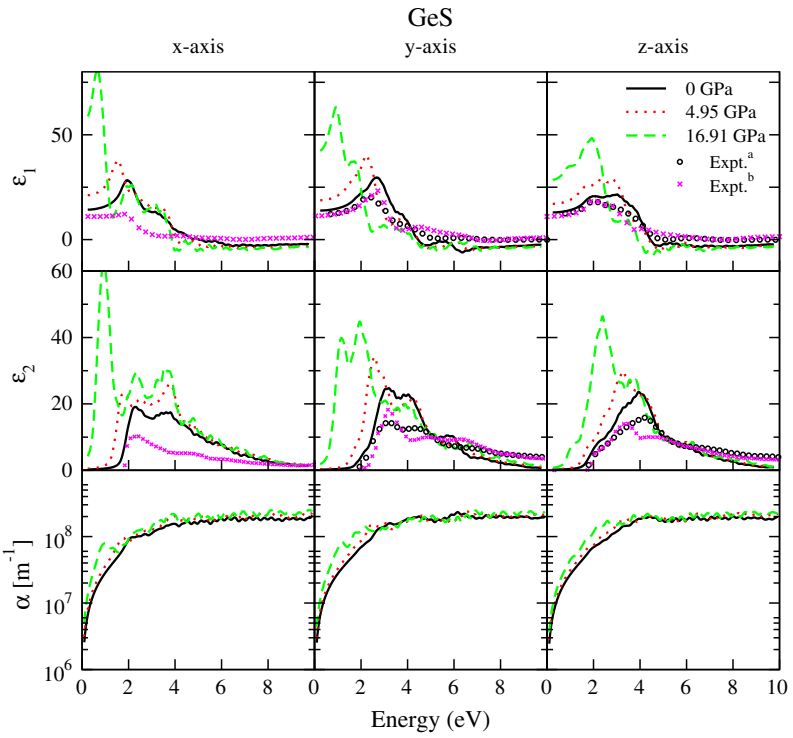

Fig. 5. Optical properties of GeS. [a]Ref. [18] and [b]Ref. [24].

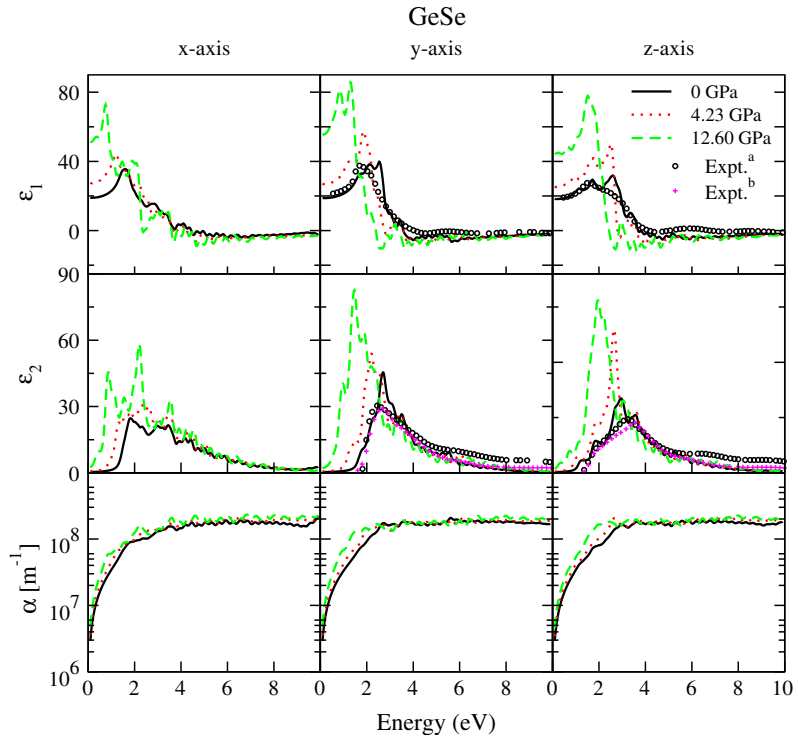

Fig. 6. Optical properties of GeSe. [a]Ref. [18] and [b]Ref. [70].

At zero pressure, the real and imaginary parts of the dielectric function show the typical response of a semiconductor with some fine structure up to ~10 eV. All four systems present a bi- and tri-axial anisotropy for different ranges of incident photon energy (e.g., ε_2 for the x-axis of α-SnS is less intense and has two main peaks, while the other two axes show a single sharp peak.

A thorough discussion of the location (in energy) and origin of the main structures of the optical properties at zero pressure was

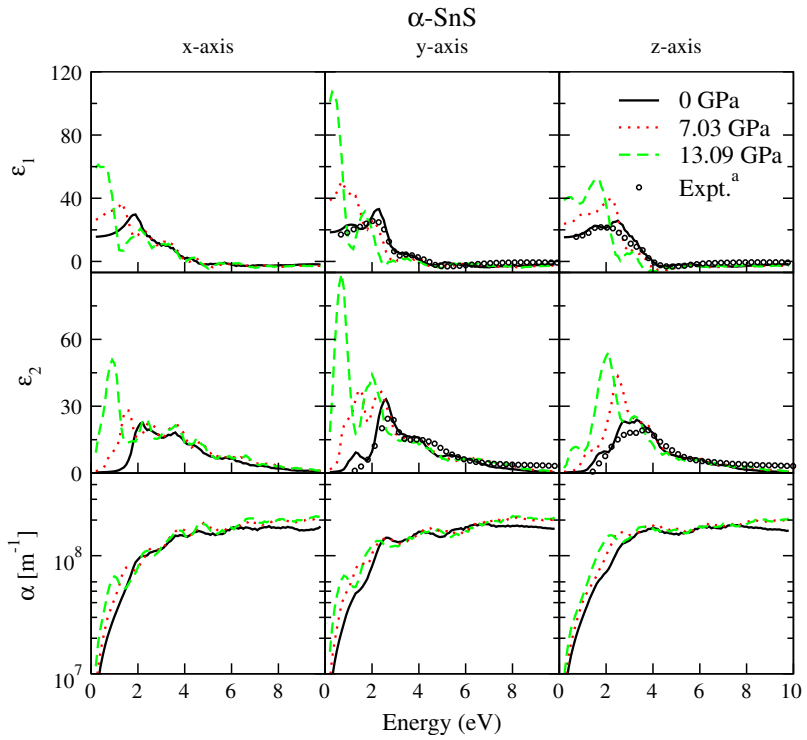

Fig. 7. Optical properties of α-SnS. [a]Ref. [18].

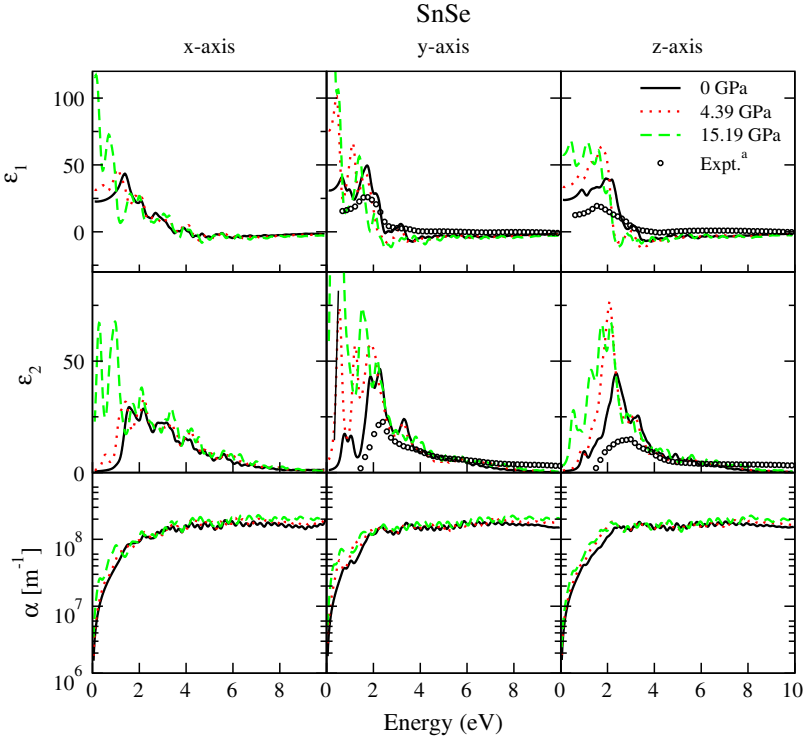

Fig. 8. Optical properties of SnSe. [a]Ref. [18].

presented in previous works [33–35]. The agreement with experimental results is quite satisfactory, in particular for ε_1 of GeS, GeSe and α-SnS. The underestimation of the gap for SnSe (discussed above) is likely to be the reason of the less satisfactory comparison of its optical properties with experiment.

As pressure increases, the static permitivity, $\varepsilon_1(0)$, rises and the main peak of ε_1 for all systems and axes becomes sharper, more intense and shifted towards lower energies. This is consistent with the broadening of the curves for ε_2 that also show an increment of the main peaks amplitude.

Correspondingly, the absorption edge of α also shifts left in energy. For energies higher than $\sim$5 eV, the optical properties show almost no change upon pressure.

4. Conclusions

We have performed what to the best of our knowledge is the first computational analysis of the band structure, densities of states and optical properties of the orthorhombic IV–VI compounds under high hydrostatic pressures, incorporating GW corrections and the electron–hole interaction through the Bethe–Salpeter equation. Our results show bi- and triaxial anisotropy for different ranges of incident photon energy and a metallization of the compounds GeS, GeSe, and SnSe upon increasing pressure. A study of the monoclinic phase of SnS (γ-SnS) should be of interest for further studies, along with a thorough experimental assessment of the phase transitions in these materials.

Acknowledgments

The authors acknowledge financial support from the Consejo Nacional de Investigaciones Científicas y Técnicas (CONICET), the Universidad Nacional de Entre Ríos (UNER) Argentina, and the Agencia de Promoción Científica y Tecnológica (ANPCyT).

References

[1] P. Dera, Introduction to High-pressure Science, High-pressure Crystallography, from Fundamental Phenomena to Technological Applications, Springer, 2009 (Chapter 1).
[2] A. Svane, N.E. Christensen, M. Cardona, A.N. Chantis, M. van Schilfgaarde, T. Kotani, Phys. Rev. B 81 (2010) 245120.
[3] P.F. McMillan, High-pressure Synthesis of Materials, High-pressure Crystallography, from Fundamental Phenomena to Technological Applications, Springer, 2009 (Chapter 30).
[4] G.R. Hearne, Nanomaterials at High Pressure: Spectroscopy and Diffraction Techniques, High-pressure Crystallography, from Fundamental Phenomena to Technological Applications, Springer, 2009 (Chapter 41).
[5] K.H.-L. Chau, R. Goehner, E. Drubetsky, H.M. Brady, W.H. Bayles Jr., P.C. Pedersen, Pressure and Sound Measurement, Measurements, Instrumentation & Sensors Handbook, CRC Press, 1999 (Chapter 26).
[6] A.F. Goncharov, J.M. Zaug, J.C. Crowhurst, E. Gregoryanz, J. Appl. Phys. 97 (2005) 094917.
[7] Z. Shi, G. Xu, P.J. McCann, X.M. Fang, N. Dai, C.L. Felix, W.W. Bewley, I. Vurgaftman, J. Meyer, Appl. Phys. Lett. 6 (25) (2000).
[8] T. Schwarzl, M. Bberl, W. Heiss, G. Springholz, J. Fnrst, H. Pascher, Proc. GMe Forum (2003) 103.
[9] M. Böberl, W. Heiss, T. Schwarzl, K. Wiesauer, G. Springholz, Appl. Phys. Lett. 82 (23) (2003).
[10] T. Schwarzl, W. Hei, G. Kocher-Oberlehner, G. Springholz, Semicond. Sci. Technol. 14 (1999) L11.
[11] J. Shan, F.C.J.M. van Veggel, M. Raudsepp, A.G. Pattantyus-Abraham, J.F. Young, in: Proceedings of the 2006 NSTI Nanotechnology Conference and Tradeshow, vol. 3, 2006.
[12] S.J. Wakeham, G.J. Hawkins, G.R. Henderson, N.A. Carthey, In: Proc. SPIE, Optics and Photonics Conference, Advances in Thin-Film Coatings for Optical Applications , vol. III, 2006, p. 62860C.
[13] T.H. Patel, R. Vaidya, S.G. Patel, Bull. Mater. Sci. 26 (6) (2003) 569.
[14] A. Agarwal, P.H. Trivedi, D. Lakshmiranayana, Cryst. Res. Technol. 40 (8) (2005) 789.
[15] R.B. Shalvoy, G.B. Fisher, P.J. Stiles, Phys. Rev. B 15 (1977) 2021.
[16] P.C. Kemeny, J. Azoulay, M. Cardona, L. Ley, IL Nuovo Cimento 39 B (2) (1977) 709.
[17] Li-Ming Yu, A. Degiovanni, P.A. Thiry, J. Ghijsen, R. Caudano, Phys. Rev. B 47 (1993) 16222.
[18] R. Eymard, A. Otto, Phys. Rev. B 16 (1977) 1616.
[19] M. Taniguchi, R.L. Johnson, J. Ghijsen, M. Cardona, Phys. Rev. 42 (6) (1990) 3634. and references therein.
[20] A. Tanuevski, Semicond. Sci. Technol. 18 (2003) 501.
[21] A.W. Parke, G.P. Srivastava, Phys. Status Solidi B 101 (1980) K31.
[22] F.M. Gashimzade, D.G. Guliev, D.A. Guseinova, V.Y. Shteinshrayber, J. Phys.: Condens. Matter 4 (1992) 1081.
[23] A.M. Elkorashy, J. Phys. C 21 (1988) 2595. and references therein.
[24] J.D. Wiley, W.J. Buckel, R.L. Schmidt, Phys. Rev. B 13 (1976) 2489.
[25] H.R. Chandrasekhar, R.G. Humphreys, M. Cardona, Phys. Rev. B 16 (1977) 2981.
[26] T. Grandke, L. Ley, Phys. Rev. B 16 (1977) 832.
[27] H.C. Hsueh, M.C. Warren, H. Vass, G.J. Ackland, S.J. Clark, J. Crain, Phys. Rev. B 53 (1996) 14806.
[28] A. Onodera, I. Sakamoto, Y. Fujii, N. Môri, S. Sugai, Phys. Rev. B 56 (13) (1997) 7935.
[29] L. Ehm, K. Knorr, P. Dera, A. Krimmel, P. Bouvier, M. Mezouar, J. Phys.: Condens. Matter 16 (2004) 3545.
[30] D. Pathinettam Padiyan, A. Marikani, Cryst. Res. Technol. 37 (11) (2002) 1241.
[31] M. Durandurdu, Phys. Rev. B 72 (2005) 144106.
[32] S. Alptekin, M. Durandurdu, Solid State Commun. 150 (2010) 870–874.
[33] L. Makinistian, E.A. Albanesi, Phys. Rev. B 74 (2006) 045206.
[34] L. Makinistian, E.A. Albanesi, J. Phys.: Condens. Matter 19 (2007) 186211.
[35] L. Makinistian, E.A. Albanesi, Phys. Status Solidi B 246 (1) (2009) 183–191.
[36] R. Laskowski, N.E. Christensen, G. Santi, C. Ambrosch-Draxl, Phys. Rev. B 72 (2005) 035204.
[37] K. Hummer, C. Ambrosch-Draxl, G. Bussi, A. Ruini, M.J. Caldas, E. Molinari, R. Laskowski, N.E. Christensen, Phys. Status Solidi B 242 (2005) 1754.
[38] G. Onida, L. Reining, A. Rubio, Rev. Mod. Phys. 74 (2002) 601.
[39] S. Baroni, S. de Gironcoli, A.D. Corso, P. Giannozzi, Rev. Mod. Phys. 73 (2001) 515.
[40] L. Hedin, S. Lundqvist, Solid State Phys. 23 (1970) 1.
[41] L. Hedin, Phys. Rev. 139 (1965) A796;
L. Hedin, S. Lundquist, in: H. Ehrenreich, F. Seitz, D. Turnbull (Eds.), Solid State Physics, vol. 23, Academic Press, New York, 1969, p. 1.
[42] L. Thomas, Proc. Camb. Philos. Soc. 23 (1927) 542.
[43] E. Fermi, Z. Phys. 48 (1928) 73.
[44] P. Hohenberg, W. Kohn, Phys. Rev. 136 (1964) 864B.
[45] X. Gonze et al., Comput. Mater. Sci. 25 (2002) 478–492.
[46] X. Gonze et al., Z. Kristallogr. 220 (2005) 558.
[47] X. Gonze et al., Comput. Mater. Sci. 180 (2009) 2582–2615.
[48] J.P. Perdew, K. Burke, M. Ernzerhof, Phys. Rev. Lett. 77 (1996) 3865;
J.P. Perdew, K. Burke, M. Ernzerhof, Phys. Rev. Lett. 78 (1997) 1396;
J.P. Perdew, S. Kurth, A. Zupan, P. Blaha, Phys. Rev. B 82 (1999) 2544.
[49] M. Fuchs, M. Scheffler, Comput. Phys. Commun. 119 (1999) 67–98.
[50] W. Kohn, L. Sham, Phys. Rev. 140 (1965) 1133.
[51] H.J. Monkhorst, J.D. Pack, Phys. Rev. B 13 (1976) 5188.
[52] D.M. Teter, G.V. Gibbs, M.B. Boisen Jr., D.C. Allan, M.P. Teter, Phys. Rev. B 52 (11) (1995) 8064.
[53] F.D. Murnaghan, Proc. Natl. Acad. Sci. USA 30 (1944) 244.
[54] F. Birch, J. Geophys. Res. 83 (1978) 1257;
F. Birch, Phys. Rev. 71 (1947) 809.
[55] E. Engel, S. Vosko, Phys. Rev. B 47 (1993) 13164;
E. Engel, S.H. Vosko, Phys. Rev. B 50 (1994) 10498.
[56] S. Drablia, H. Meradji, S. Ghemid, S. Labidi, B. Bouhafs, Phys. Scr. 79 (2009) 045002.
[57] M. Dadsetani, A. Pourghazi, Optical Comm. 266 (2006) 562–564.
[58] N.E. Christensen, K. Hummer, C. Ambrox-Draxl, Phys. Rev. B 71 (2005) 081202-1.
[59] F. Ladstädter, U. Hohenester, P. Pusching, C. Ambrosch-Draxl, Phys. Rev. B 70 (2004) 235125-1.
[60] B. Arnaud, M. Allouani, Phys. Rev. B 63 (2001) 085208;
B. Arnaud, M. Alouani, Phys. Rev. B 62 (2000) 4464.
[61] E.A. Albanesi, W.L. Lambrecht, B. Segall, J. Vac. Sci. Technol. B 12 (1994) 2470.
[62] R.D. Sole, R. Girlanda, Phys. Rev. B 48 (1993) 11789.
[63] S. Wey, A. Zunger, Phys. Rev. B 55 (1977) 13605.
[64] E.E. Salpeter, H.A. Bethe, Phys. Rev. B 84 (1951) 1232.
[65] R. Haydock, Comput. Phys. Commun. 20 (1980) 11.
[66] G.V. Vajenine, X. Wang, I. Efthimiopoulos, S. Karmakar, K. Syassen, M. Hanfland, Phys. Rev. B 79 (2009) 224107.
[67] S. Radescu, A. Mujica, J. López-Solano, R.J. Needs, Phys. Rev. B 83 (2011) 094107.
[68] D. Vogel, P. Krnger, J. Pollmann, Phys. Rev. B 54 (1996) 5495.
[69] M. Parenteau, C. Carlone, Phys. Rev. B 41 (1990) 5227.
[70] G. Valiukonis, F.M. Gashimzade, D.A. Guseinova, G. Krivaitė, A.M. Kulibekov, G.S. Orudzhev, A. Šileika, Phys. Status Solidi B 117 (1983) 81.